Deformation and Noise Mitigation for the Linear Switched Reluctance Motor With Skewed Teeth Structure

Yu Zou,[1,2] Ka-Wai Eric Cheng,[2] Norbert C. Cheung,[2] and Jianfei Pan[1]

[1]Shenzhen Key Laboratory of Electromagnetic Control, Shenzhen University, Shenzhen 518060, China
[2]Department of Electrical Engineering, Hong Kong Polytechnic University, Hong Kong

In this paper, a skewed teeth structure is proposed for the linear switched reluctance motor (LSRM). First, the normal force, as the main source of the machine deformation as well as the acoustic noise, is analyzed theoretically. Second, the skewed LSRM is designed, and the angle of the skewed structure is analyzed and optimized. Then, the normal force output of the LSRM is calculated using the finite element method (FEM), and the deformation results for the proposed machine are obtained. The relationship of the normal force and the skewed angle is derived. Finally, the experimental results demonstrate that the acoustic noise is reduced, which is a testament to the effectiveness of the proposed structure.

***Index Terms*— Acoustic noise, deformation, finite element method (FEM), linear switched reluctance motor (LSRM), skewed structure.**

I. Introduction

LINEAR switched reluctance motors (LSRMs), as one type of direct-drive actuator, are characterized by simple machine structures, low cost and high robustness. LSRMs have no permanent magnets and are capable of operation under hostile environments. A typical example is to apply the LSRMs as the control objects for the high-precision position control applications. Normally, both the stator and the mover employ the doubly salient teeth structure, which inevitably leads to normal force fluctuations during either single or multiple phase current excitations. Normal force fluctuations, as one of the main causes for motor deformation, further generate acoustic noise during the operation process [1].

To reduce the acoustic noise of the motors, some advanced linearization schemes and control strategies are employed for LSRMs [2], [3], including the force distribution function, parameter identification and self-tuning control, and so on. In [5], the proposed method is dedicated to the calculation of the acoustic noise based on the spectrum analysis, and [6] presents a simple way to test acoustic noise for the rotary switched reluctance motor (RSRM) under different working conditions. Some approaches are focused on the optimization of the excitation strategy to decrease the change rate of the normal force. In [7], a method to mitigate the vibration through twice turning OFF the power switches of the drive for the RSRM is introduced. In [8], the intelligent current profile for radial force modification is employed to decrease the acoustic noise of the RSRM. Due to the inherent mechanical characteristics from the rotor and stator teeth structure, the noise and deformation caused by the sharp change of normal forces between the rotor and stator teeth can no longer be reduced by the methods discussed above. In addition, they only apply to certain operational conditions.

On the other hand, the design of improved mechanical structures of switched reluctance motor s also plays a key role for acoustic noise reduction. In [9], the modal analysis for the motor is presented, and the radiating rib structure is designed to reduce the radial force and decrease the acoustic noise. The non-uniform air-gap structure is proposed in [10] for a single-phase RSRM for high-speed operations. The stator pole structure is further optimized for the adaptation to the air gap to mitigate the acoustic noise [11]. In [12], the skewed structure is proposed for a single-phase RSRM for noise reduction. The design methodology of the skewed structure for the stator and rotor teeth is presented to reduce the acoustic noise and motor vibration by analyzing the distribution of the radial force. However, the specific relationship between the radial force and the skew angle is not investigated.

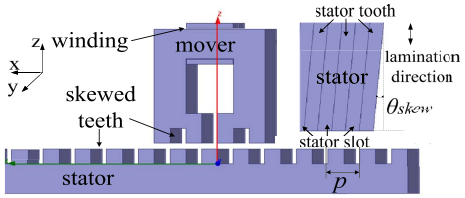

Fig. 1. LSRM with skewed teeth structure.

In this paper, the skewed structure for the LSRM is proposed to reduce the deformation and noise for the motor. Both the stator and mover adapt to the skewed structure and the normal force is analyzed theoretically. Not only the deformation of the motor is calculated using the finite element method (FEM), but the relationship of the normal force to the skewed angle is analyzed and derived. The skewed angle is optimized and the deformation is mitigated as well. The experimental platform is constructed to measure the acoustic noise of the LSRMs. Both the simulation results of the deformation and the acoustic noise tests verify the effectiveness of the skewed structure for the LSRM.

II. Structure and Analysis

A. Mechanical Structure

The LSRM is mainly composed of three movers and a stator, which are fixed on an aluminum board. The movers with three phases are stacked by laminated silicon steels and assembled in the moving platform. Each phase has a concentrated winding connecting to the drives [13]. The same skewed structure for both the stator and rotor teeth is employed, as shown in Fig. 1, for any one phase.

Manuscript received February 21, 2014; revised April 14, 2014 and April 30, 2014; accepted May 2, 2014. Date of current version November 18, 2014. Corresponding author: J. Pan (e-mail: pan_jian_fei@163.com).

Color versions of one or more of the figures in this paper are available online at http://ieeexplore.ieee.org.

Digital Object Identifier 10.1109/TMAG.2014.2323420

B. Mathematic Model

The LSRM is a typical electromechanical device with three-phase electrical input ports and one mechanical output port. The dynamic equation of the LSRM can be expressed as [1]

$$F = M \cdot \frac{d^2x}{dt^2} + D \cdot \frac{dx}{dt} + f \tag{1}$$

where F stands for the electromagnetic force along the x-direction, M is the total mass of the moving platform, D is the damping coefficient, x is displacement, and f represents the load force. From the electrical part, for any one phase

$$u_j = R_j \cdot i_j + \frac{d\lambda_j}{dt} (j = A, B, C) \tag{2}$$

where u_j, i_j, R_j, and λ_j represent voltage drop, current, resistance, and flux-linkage for any one phase.

C. Normal Force Generation

According to the Maxwell tensor method, the normal force $\vec{F}$ can be calculated by [12]

$$\vec{F} = \int_s \vec{T} ds \tag{3}$$

where s is the integral area and $\vec{T}$ is the Maxwell stress tensor with

$$\vec{T} = \frac{1}{\mu_0}\left[(\vec{B} \cdot \widehat{n})\vec{B} - \frac{1}{2} \cdot \nabla \vec{B}^2 \cdot \widehat{n}\right]. \tag{4}$$

The normal force in the unit area can be expressed as

$$\vec{F}_n = \frac{1}{2\mu_1}(\vec{B}_{1n}^2 - \vec{B}_{1t}^2) - \frac{1}{2\mu_2}(\vec{B}_{2n}^2 - \vec{B}_{2t}^2) \tag{5}$$

where $\vec{F}_n$ is the force element of the vertical direction. μ_0 is the relative permeability of vacuum. $\vec{B}$ is the magnetic intensity. $\widehat{n}$ is the normal vector of the vertical direction. μ_1, $\vec{B}_{1n}$, $\vec{B}_{1t}$ and μ_2, $\vec{B}_{2n}$, $\vec{B}_{2t}$ are the relative permeability, magnetic intensity from the vertical direction, and tangential direction for different materials 1 (air) and 2 (silicon steel), respectively. The deformation and acoustic noise are mainly generated by the magnetic normal force along the z-axis [1].

D. Electromagnetic Characteristics

The magnetic field distribution for any one excitation phase is shown in Fig. 2(a). Since the mover, the corresponding stator and the air gap region form a short magnetic path, mutual coupling can be neglected between any phases [2]. The self-inductance profile of one phase under different phase current levels and the propulsion force waveforms in the x-direction according to displacement can be found in Fig. 2(b) and (c), respectively.

III. Determination of the Skew Angle

A. Analysis of the Skew Angle

The skewed teeth structure can be found in Fig. 3 with main machine parameters tabulated in Table I. Assuming that the thickness of the lamination is l_1 and the stack length l, then the skew angle θ_{skew} can be derived as

$$\tan\theta_{skew} = \frac{l_3}{l} = \frac{l_2}{l_1}. \tag{6}$$

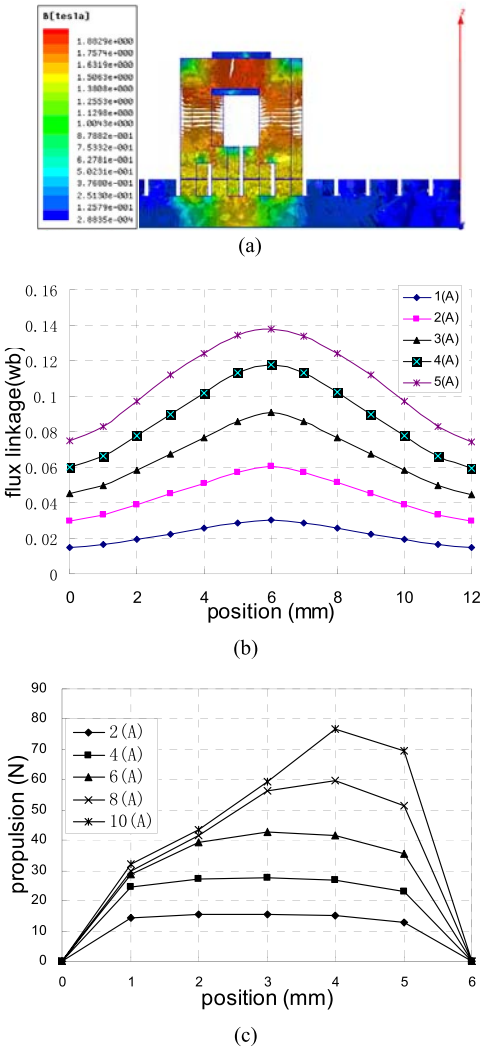

Fig. 2. (a) Flux distribution. (b) Flux-linkage. (c) Propulsion force.

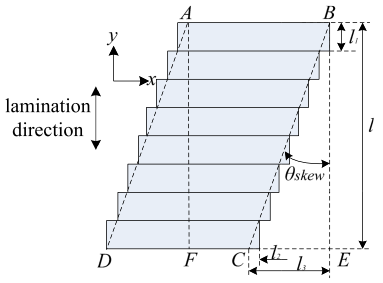

Fig. 3. Lamination structure of the poles.

The pole area of the skewed structure is the enclosed area denoted by ABCD. Although area ABCD equals area ABEF, the distribution of the normal force is different. It can be seen that the normal force distributes along line AD and line AF for the skewed structure and the vertical structure, respectively. Accordingly, we can define the line density of the normal force as

$$\varepsilon = \frac{F_z \cdot cos\theta_{skew}}{l} (0 \le \theta_{skew} \le 90). \tag{7}$$

It can be concluded that ε decreases with the increased skew angle.

TABLE I
MAJOR SPECIFICATIONS

PARAMETER	QUANTITY
Rate power	150 W
Rate current	10 A
Pole width ($p/2$)	6 mm
Pole pitch (p)	12 mm
Phase division	10 mm
Phase resistance	2 ohm
Air gap length	0.3 mm
Number of turns	160
Stack length of the motor	50 mm
Height of the lamination steel	0.5 mm
Material type	50W1300
Thickness of laminations	0.5 mm
Skew angle	20 degree

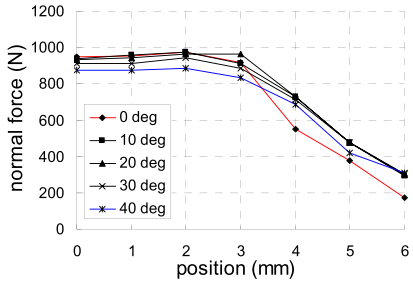

(a)

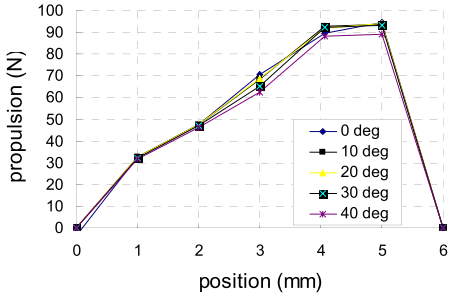

(b)

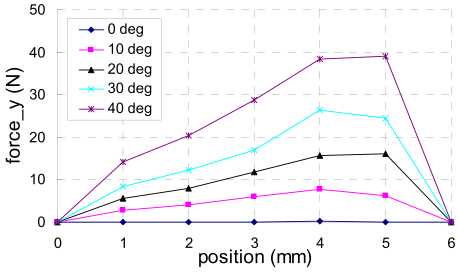

(c)

Fig. 4. (a) Normal force profile versus position at rated current. (b) Propulsion force with respect to skew angle at different positions. (c) Force output along y-axis versus position.

B. Optimization of the Skew Angle

The normal force along the z-axis is calculated using the 3-D FEM. The normal force of one phase at the rated current excitation from the aligned position (0 mm) to the unaligned position (6 mm) is derived, as shown in Fig. 4(a). It is clear that the disparities between the maximum normal force values (at 0 mm) and its minimal values (at 6 mm) decrease as the skew angle is increased. At the rated current excitation, the relationship between the propulsion force and the deformation angle is shown in Fig. 4(b). It can be concluded from the simulation results that the influence of the skew angle on the propulsion force can be neglected.

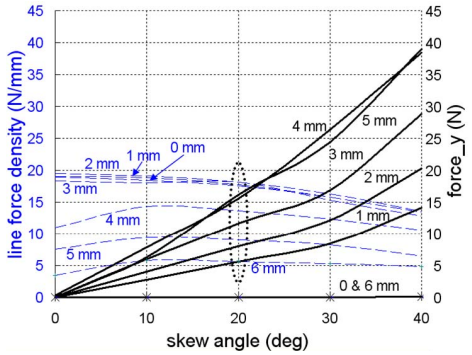

Fig. 5. Force output along the y-axis (black), and the line density of the normal force (blue).

On the other hand, the skewed pole structure not only generates the propulsion force along the x-axis, but it also produces the force along the y-axis, which should be counterbalanced by the linear guides when any phase is excited. The force from the y-axis at the rated current excitation at different skew angles according to positions can be found in Fig. 4(c). It can be seen that the maximum force output along the y-axis appears at the position of 4–5 mm and that y force is approximately proportional to the value of the skew angle. The values of the line density ε with respect to the skew angle at different positions are also calculated, as the blue profiles shown in Fig. 5. It can be concluded that with the increasing of the skew angle, the value of ε decreases at each position, except that the skew angle is zero. This indicates that the change rate of the normal force is also reduced as the skew angle is increased.

If the profiles of the line density of the normal force and the force output from y-axis are plotted together, as shown in Fig. 5, the selection of the skew angle is considered for the following reasons.

1) When the skew angle exceeds 10°, the line density of the normal force will decrease if the skew angle increases. Nevertheless, the difference of the normal force at the aligned and unaligned positions becomes small.
2) When the skew angle exceeds 30°, the force output from the y-axis increases dramatically.
3) To reduce the deformation and mitigate the acoustic noise, the normal force profiles should be smooth enough according to different positions, and this means that the disparities should be kept as small as possible.

Since the force output along the y-axis increases with the value of the skew angle, to reduce the burden on the linear guides, the skew angle is selected as 20° for the LSRM.

IV. SIMULATION AND EXPERIMENTAL TEST

A. Simulation of Deformation

After the determination of the skew angle, the deformation simulation of the stator is performed for the LSRM with the skewed pole and non-skewed pole structure with the same dimensions and ratings in ANSYS FEM environment. The analysis is based on the condition that the moving part is perfectly fixed with no deformation. All the lamination plates are stacked together and fixed by two supporting aluminum

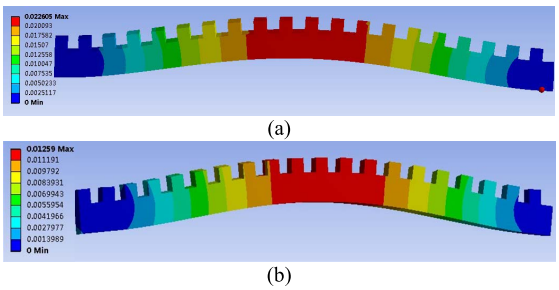

Fig. 6. Deformation of the LSRM with (a) non-skewed angle and (b) skewed pole structure.

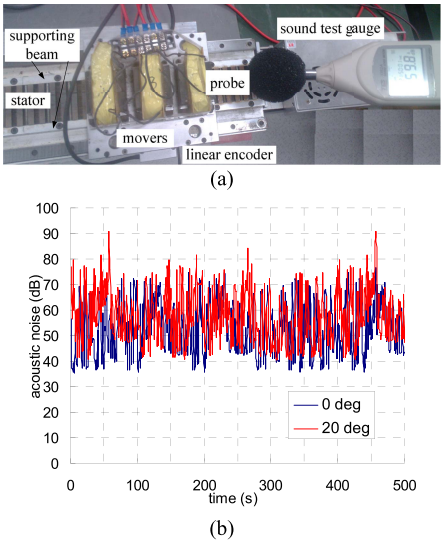

Fig. 7. (a) Experimental setup. (b) Test results.

beams, which are fastened to the stator base with screws. As the same phase is excited with the rated current for 1 s, the deformation contours for the LSRM with the skewed structure and non-skewed structure at the same position (0 mm) can be found in Fig. 6(a) and (b), respectively. The maximum deformation displacement of the skewed structure is less than 0.013 mm, which is approximately half of that from the non-skewed structure. The simulation results indicate that the normal force from the skewed structure is exercised on the stator evenly.

B. Acoustic Noise Test

The experiment is constructed under the dSPACE DS1104 control environment with three commercial current amplifiers to operate the LSRM in the velocity control mode based on the proportional integral differential algorithm [2]. For performance comparison between the LSRMs with the skewed structure and non-skewed structure, all control parameters are regulated as the same values. An acoustic noise test gauge is employed with the sampling rate of 1 s and the whole experiment is operated in real-time, as shown in Fig. 7(a), for the experimental setup.

The test profiles of acoustic noise according to time are drawn in the same figure at the operation speed of 0.5 m/s. It can be seen from Fig. 7(b) that the transient noise of the skewed LSRM is less than the values from the non-skewed LSRM, which attests to the effectiveness of the proposed machine structure. It can be also calculated that the mean noise values over the experimental measurement for the skewed and non-skewed LSRM can be calculated as 53 and 58 dB, respectively, with a difference of 5 dB.

V. Conclusion

A skewed teeth structure is proposed for the LSRM. The skew angle for the LSRM is designed and optimized. Deformation simulation and experimental acoustic noise test results demonstrate the effectiveness of the proposed structure.

It is concluded that the skewed structure generates more force in the y-direction and influences the machine performance. It is suggested that more research be carried out to counterbalance the generated force with some advanced control strategies and improved mechanical structures. It is expected that this type of LSRM can be used for industrial applications in the future.

Acknowledgment

This work was supported by the National Natural Science Foundation of China under Project 51007059, the Guangdong Natural Science Foundation under Project S2011010001208, and Shenzhen government under Project Code of JCYJ20130329144017199.

References

[1] J. F. Pan, Y. Zou, and G. Cao, "An asymmetric linear switched reluctance motor," *IEEE Trans. Energy Convers.*, vol. 28, no. 2, pp. 444–451, Jul. 2013.

[2] J. F. Pan, N. C. Cheung, and Y. Zou, "An improved force distribution function for linear switched reluctance motor on force ripple minimization with nonlinear inductance modeling," *IEEE Trans. Magn.*, vol. 48, no. 11, pp. 3064–3067, Nov. 2012.

[3] S. W. Zhao, N. C. Cheung, W.-C. Gan, J. M. Yang, and J. F. Pan, "A self-tuning regulator for the high-precision position control of a linear switched reluctance motor," *IEEE Trans. Ind. Eletron.*, vol. 54, no. 5, pp. 2425–2434, Oct. 2007.

[4] T. Jintanawan, A. Sillapapinij, and N. Ajavakom, "Effects of tolerance design on suppression of electromagnetic-induced acoustic noises and vibration transmission in hard disk drive spindle motors," *IEEE Trans. Magn.*, vol. 45, no. 11, pp. 5129–5134, Nov. 2009.

[5] J. O. Fiedler, K. A. Kasper, and R. W. De Doncker, "Calculation of the acoustic noise spectrum of SRM using modal superposition," *IEEE Trans. Ind. Eletron.*, vol. 57, no. 9, pp. 2939–2945, Sep. 2010.

[6] C. Lin and B. Fahimi, "Prediction of radial vibration in switched reluctance machines," *IEEE Trans. Energy Convers.*, vol. 28, no. 4, pp. 1072–1081, Dec. 2013.

[7] Z. Q. Zhu, X. Liu, and Z. Pan, "Analytical model for predicting maximum reduction levels of vibration and noise in switched reluctance machine by active vibration cancellation," *IEEE Trans. Energy Convers.*, vol. 26, no. 1, pp. 36–45, Mar. 2011.

[8] J. Y. Chai and C. M. Liaw, "Reduction of speed ripple and vibration for switched reluctance motor drive via intelligent current profiling," *IET Electr. Power Appl.*, vol. 4, no. 5, pp. 380–396, May 2010.

[9] J. Sun, Q. Zhan, S. Wang, and Z. Ma, "A novel radiating rib structure in switched reluctance motors for low acoustic noise," *IEEE Trans. Magn.*, vol. 43, no. 9, pp. 3630–3637, Sep. 2007.

[10] D.-H. Lee, T. H. Pham, and J.-W. Ahn, "Design and operation characteristics of four-two pole high-speed SRM for torque ripple reduction," *IEEE Trans. Ind. Eletron.*, vol. 60, no. 9, pp. 3637–3643, Sep. 2013.

[11] Y. K. Choi, H. S. Yoon, and C. S. Koh, "Pole-shape optimization of a switched-reluctance motor for torque ripple reduction," *IEEE Trans. Magn.*, vol. 43, no. 4, pp. 1797–1800, Apr. 2007.

[12] H.-Y. Yang, Y. C. Lim, and H. C. Kim, "Acoustic noise/vibration reduction of a single-phase SRM using skewed stator and rotor," *IEEE Trans. Ind. Eletron.*, vol. 60, no. 10, pp. 4292–4300, Oct. 2013.

[13] J. F. Pan, Y. Zou, and G. Cao, "Adaptive controller for the double-sided linear switched reluctance motor based on the nonlinear inductance modeling," *IET Electr. Power Appl.*, vol. 7, no. 1, pp. 1–15, Jan. 2013.